THOMSON SCATTERING DIAGNOSTIC IN THE BOUNDARY LAYER OF ASDEX

H. Murmann, M. Huang[+]

IPP III/95 July 1983

MAX-PLANCK-INSTITUT FÜR PLASMAPHYSIK

8046 GARCHING BEI MÜNCHEN

MAX-PLANCK-INSTITUT FÜR PLASMAPHYSIK

GARCHING BEI MÜNCHEN

THOMSON SCATTERING DIAGNOSTIC IN THE BOUNDARY LAYER OF ASDEX

H. Murmann, M. Huang[+]

IPP III/95 July 1983

[+]On leave from Academia Sinica, Peking, The People's Republic of China

Die nachstehende Arbeit wurde im Rahmen des Vertrages zwischen dem Max-Planck-Institut für Plasmaphysik und der Europäischen Atomgemeinschaft über die Zusammenarbeit auf dem Gebiete der Plasmaphysik durchgeführt.

IPP III/95 H. Murmann
M. Huang+

THOMSON SCATTERING DIAGNOSTIC IN THE BOUNDARY LAYER OF ASDEX

July 1983

Abstract

The divertor experiment ASDEX has been equipped with a Thomson scattering system, designed to measure radially resolved electron temperature and density profiles in the boundary layer between the hot plasma core and the wall. Thus, it is possible to obtain detailed information about plasma edge phenomena as a basis of divertor physics. The measured electron temperature at the magnetic separatrix can be described by the Coppi-Mazzucato scaling law for the electron heat conductivity in ohmically heated plasmas. This is analyzed over a wide range of ASDEX plasma parameters and discharge conditions. During additional heating by neutral injection the Te-profiles show a steepening in the scrape-off area, which can be a consequence of a local decrease in thermal conductivity responsible for the good energy confinement observed for "H"-regime discharges.

+On leave from Academia Sinica, Peking, The People's Republic of China

CONTENTS

Thomson scattering diagnostic in the boundary layer

1. Introduction

The investigation of particle and energy transport phenomena is crucially depending on the knowledge of electron density and temperature and their radial gradients in the boundary layer separating the bulk plasma from material walls. Because of the high energy fluxes Langmuir probes can only be operated far in the shadow of limiters, so the installation of an additional laser scattering system was favored on ASDEX, designed primarily to measure the properties of the cold, low density plasma edge with steep radial gradients. Special emphasis was put on:

- small scattering volumes to increase spatial resolution and consequently the use of a high power, low divergence laser, focussed on the plasma edge
- high overall transmission of the detection optics
- high dynamic range to cover the expected T_e and n_e regimes also during additional heating.

2. Technical description

A schematic representation of the scattering system is shown in Fig. 1. The beam (12 J/20 ns, divergence $\lesssim$1 mrad) of a Q-switched ruby laser/1/ is focussed (f = 100 cm) in the equatorial plane of the plasma, so that over a region of $\Delta r \sim 6$ cm in the plasma edge the beam diameter is less than 1 mm. The beam leaves the vacuum vessel through a Brewster-window and is absorbed into a beam dump. A small fraction of the transmitted laser light is used for monitoring purposes. Comparison with the beam power measured before the entrance into the vessel is done automatically after each shot and is an effective control of laser power stability, alignment and transmission of the vacuum windows.

The observation optics (f/3.5) oriented at an angle of 122° to the laser beam consists of 5 interference filter polychromators of 3 spectral channels each. The detectors are oriented perpendicular to each other making use of polarizing optics /2/ in very compact arrangement.

The scattered light is detected by photomultipliers which have a selected quantum efficiency of $\gtrsim$7 % at 700 nm /3/. Since the relatively high noise level in the environment of a tokamak can only be partly shielded out by copper and iron castings, the signals are amplified by a factor of 10 via a fast, low noise integrated amplifier. The scattered light signals, as well as the quasi DC plasma light background are measured and integrated by a fast ADC (CAMAC) for 32 gated time intervals of 60 ns width centered about the laser pulse. By this means it is possible to measure the average plasma light fluctuation level which crucially limits the accuracy of the measurement at low densities.

The system was absolutely calibrated with a tungsten ribbon lamp with known colour temperature and Rayleigh-scattering in argon. To be able to compensate numerically for a loss of transmission of the observation windows due to impurity particle radiation, the transmission of the detection optics is monitored automatically after each shot by means of a light beam that shines from within the vacuum vessel through the optics. The stability of the detection electronics can be monitored by the flash of a light diode array.

Summary of technical data

laser:	6943 Å, 12 J, 20 ns, $\lesssim$1 mrad
spectrometer type:	interference filter/polarizing optics 3 channels per spatial point
spatial region:	5 local points/simultaneous measurement; $\Delta r \sim 1$ cm 0,87 < r/a < 1,03 (for a centered plasma, r = 40 cm, R = 165 cm)
location:	equatorial plane 199 cm $\leq$ R $\leq$ 206 cm
temperature range:	2 eV < T_e < 1000 eV
density range:	$n_e \geq 5 \cdot 10^{11}$ cm^{-3}

3. Results

The typical output of a CAMAC ADC is shown in Fig. 2 for two low density cases, the upper being at the detection limit. As the spectral width of the interference filter channels is relatively small ($\int_{\Delta\lambda} T(\lambda)d\lambda \approx 10...20$ Å, T: Transmission, $T_{peak} \approx 60$ %) and the gate time is short ($t_{gate} \approx 3t_{laserpulse}$) the plasma background level is usually small compared to the signal (3...10%). An essential limitation to the detection level, however, is given by the fluctuation of the plasma light which may be more than an order of magnitude above the bremsstrahlung noise. Thus the lowest electron density equivalent to S/N ~ 1 is about $5 \cdot 10^{11}$ cm^{-3}. The problem of parasitic light of the laser-wavelength can be overcome by the use of selected interference filter sets with suppression of the laser wavelength more than 10^5 at a spectral distance of 2 ... 3 times the half width of the filter.

Figure 3 shows spectra delivered by the 5 spatial channels from a standard discharge. The actual spectral shapes of the transmission functions $T(\lambda)$ of the interference filter channels are taken into account numerically by an iteration procedure. The measured scattering signals are compared with the calculated scattered laser power $\int F(T_e,\lambda)\ T(\lambda)\ d\lambda$ that passes through a detection channel, where $F(Te,\lambda)$ is the scattering function. Generally it is observed, that the spectra deviate slightly from a linear decay which can be partly attributed to the finite scattering volume of 1 cm radial depth. The calculated "temperature" is then to be understood as average energy per electron and found from an average slope of the function log Q versus $\Delta\lambda^2$ in Fig. 3. This effect is the more critical when T_e and n_e are low, and high gradients prevail within the observation area of a polychromator. Under certain plasma conditions, however, one observes appreciable deviations from linearity which cannot be explained as above, and the existence of a non-Maxwellian electron velocity distribution must be assumed in the presence of steep profile gradients.

3.1 Profile measurements

Figure 4 shows the temporal evolution of T_e and n_e at 5 fixed positions within the torus for a divertor discharge, with about 3 MW neutral beam power injected during the time interval 1.1 s < t < 1.3 s. H_α light emission, as detected in a divertor chamber is also plotted on the same

time scale, marking the transition of the discharge from ohmic heating to beam heating with low β_p (L-phase) and finally to a state with high β_p (H-phase). During the L phase T_e rises steadily, n_e drops slightly at the beginning. During the H-phase a sudden onset of H_α-light bursts is observed at about t ~ 1.2 s when the discharge changes from a quiet to a turbulent period, which is clearly reflected in the T_e and n_e profiles in the boundary layer from that time on, when sudden fluctuations occur and data scatter appreciably.

It has to be noted that the temporal behavior of the profiles as displayed in Fig. 4 , is masked by an outward movement of the plasma during neutral beam heating due to enhanced β_p, while the observation volumes of the Thomson scattering device remain fixed. This problem can be overcome if a relative radius $\Delta r = r - r_s$ is introduced. This is shown in Fig. 5, where T_e and n_e are plotted versus Δr for 3 characteristic discharge times: 1.05 s (ohmic heating alone), 1.15 s (L-phase) and 1.25 s (H-phase) for a series of slightly different radial positions to increase the spatial resolution of the laser system.

3.2 Electron temperature and density near the separatrix

As shown in a previous paper /4/, the electron temperature $T_e(o)$ in the plasma center depends on the safety factor q_a, the toroidal magnetic field B, Z_{eff} etc. The dependence on the average line density was found to be weak on ASDEX.

At the plasma edge $T_e(r \sim a)$ does also clearly depend on q_a and $\bar{n}_e$ as shown in Fig. 6, where several T_e-profiles are plotted versus $\Delta r = r - r_s$ for typical q_a and $\bar{n}_e$ values in stationary plasmas. The density dependence is apparently higher at low values of q_a. Again the location of the separatrix was calculated from magnetic flux measurements.

When neutral beam heating is applied, one observes a steady increase of the boundary temperature inside the separatrix. In the scrape-off layer $r > r_s$, T_e does not rise to the same extent as expected in this open field line area. This is shown in Fig. 7 for a low q_a discharge with

$\bar{n}_e = 2 \cdot 10^{13}$ cm^{-3} average line density. The heating power in this series of discharges was varied between ~0.4 MW ohmic heating alone and ≈3 MW neutral beam additional heating. The location of the separatrix was calculated as above and revealed an outward shift with rising β_{pol}. At the highest applied heating power, the separatrix temperature of the electron reaches about 100 ... 150 eV. At lower power levels $T_e(r = r_s)$ becomes 50 ... 100 eV depending on q_a and $\bar{n}$.

As mentioned above, the character of the T_e profiles does not alter markedly in the scrape-off layer $r > r_s$ and can be described by an exponential decay function with an amplitude depending on input power, q_a and $\bar{n}$:

$$T_e(r) = T_e(r_s) \cdot \exp\{(r_s - r)/\lambda_T\} \qquad \text{for } r \geq r_s$$

The e-folding length, λ_T, is about 1 cm for ohmic heating and decreases to about 0.7 cm at 3 MW additional heating (see Fig. 8). This confirms the theoretical prediction, that the electron energy transport is dominated by heat conduction parallel to the magnetic field in the plasma edge, as stated in paper /5/.

The electron density profile can also be described by an exponential function as $T_e(r)$:

$$n_e(r) = n_e(r_s) \exp\{(r_s - r)/\lambda_n\} \qquad \text{for } r \geq r_s$$

The decay length λ_n is typically 1.5 ... 2 cm and shows no dependence on heating power, q_a, $\bar{n}_e$ etc. within the error bars. In the case of ungettered divertor discharges the amplitude $n_e(r)$ depends linearly on the average line density $\bar{n}_e$ for $\bar{n}_e \lesssim 0.3 \cdot 10^{14}$ cm^{-3} and stronger than linear for densities above (Fig. 9). This deviation from linearity is not observed, or much smaller, for Ti-gettered discharges. Thus the density profiles become broader with rising line averaged density $\bar{n}$, when getter pumps are not in action. In this case the separatrix density can be approximated by

$$n_e(r_s) \approx 0{,}2 \ldots 0{,}3\ \bar{n}_e \qquad \text{(OH, NBI(H))};$$

the proportionality factor is slightly lower in the NBI(L) phase.

4. Electron heat conduction in the boundary region

Energy losses from the hot plasma core are dominated by heat conduction /4/, convection does not play an important role. The same statement is found to be valid for the boundary layer outside the separatrix, as analyzed in paper /5/. But in contrast to the region $r < a$, at $r > a$ the loss is dominated by conduction parallel to the magnetic field, which obviously causes the sudden change in the character of the $T_e(r)$ profile at $r \sim a$ (Fig. 6). If the convection term is negligible one can write the balance equation for the power per unit length in the ohmic heated phase as:

$$P_{OH}(r) = P_e(r) + P_i(r) + P_{rad}(r) \tag{1}$$

with

$$P_{OH}(r) = \int_0^r 2\pi r' dr' j(r') \cdot E;$$

$$P_e(r) = -2\pi r \quad \kappa_e \frac{\partial kT_e}{\partial r} = -2\pi r \, n_e \chi_e \frac{\partial kT_e}{\partial r};$$

$$P_i(r) = -2\pi r \quad \kappa_i \frac{\partial kT_i}{\partial r} = -2\pi r \, n_i \chi_i \frac{\partial kT_i}{\partial r};$$

$$P_{rad}(r) = \int_0^r p_{rad}\Big|_{local} \, 2\pi r' dr'.$$

where E is the electric field and assumed to be independent on r, P_{OH} is the ohmic heating power, $P_{e,i}$ the power lost by electron and ion heat conduction, P_{rad} the power lost by radiation, $\kappa_{e,i}$, $\chi_{e,i}$ are heat conductivity and diffusivity respectively. From these equations the heat diffusivity for the electrons can be derived:

$$\chi_e(r) = \frac{P_{OH}(r) - P_{rad}(r) - P_i(r)}{-2\pi r \, n_e \frac{\partial kT_e}{\partial r}} \tag{2}$$

The denominator consists of measurable quantities, the numerator can be simplified in the outer plasma zone, when most of the ion heat content is transferred back to the electrons again, i.e. ion heat conduction losses can be neglected. $P_{OH}(r) = E \cdot j(r)$; the current density can be calculated from Spitzer law: $j(r) \sim T_e^{3/2}(r)$. So equ. (2) becomes

$$\chi_e(r) \sim \frac{P_{OH}(r) - P_{rad}(r)}{-2\pi r\, n_e \frac{\partial kT_e}{\partial r}} \qquad \text{for } r \lesssim a \qquad (3)$$

This is demonstrated in Fig. 10, where the power-fluxes P_{OH}, P_i, P_{rad} and $P_e = P_{OH} - P_i - P_{rad}$ are plotted versus the minor plasma radius for a standard discharge of medium density; P_{rad} is measured by bolometry, the ion diffusivity χ_i is assumed to be neoclassical according to Galeev and Sagdeev

$$\chi_i(r) = \chi_{io} \frac{q(r)\, T_i^{3/2}(r)}{R\, B^2}$$

T_i is measured in the plasma center; the profile is assumed to be proportional to $n_e(r)$. Obviously at the plasma edge the ohmic heating power is mainly dissipated by electron heat conduction and radiation.
The balance equation is then reduced to

$$-2\pi r \chi_e n_e \frac{\partial kT}{\partial r} = P_e = E \cdot I(r)\ (1 - \frac{P_{rad}}{P_{OH}}). \qquad (4)$$

With the Coppi-Mazzucato scaling law for the electron heat diffusivity /6/

$$\chi_e(r) \sim B_\varphi\, n_e^{-0,8}(r)\, q^{-1}(r)\, T_e^{-1}(r)$$

and the usual definition of the cylindrical q value

$$q(\rho) = q_a\, \rho^2\, I(a)/I(\rho); \qquad \rho = r/a$$

one arrives at the differential equation

$$-2\pi\ \chi_o\ B_\varphi\ n_e^{1/5}\ \frac{1}{q_a}\cdot\frac{1}{T_e}\ \frac{\partial T_e}{\rho\,\partial\rho} = P_{OH}(a)\ [1 - P_{rad}/P_{OH}] \qquad (5)$$

The fraction P_{rad}/P_{OH} of the total power lost by radiation is usually small in the center and about 20 % at the plasma edge /7/ for typical ASDEX discharges (see Fig. 10) and the right hand side of equ. (5) can be approximated by

$$P_{OH}(a)\ [1 - P_{rad}/P_{OH}] \approx P_{OH}(a)\ (1 - \alpha\ \rho^2) \qquad (6)$$

with $\alpha \approx 0.2$

With this substitution and the approximation that $n_e^{1/5}(\rho)$ is a weak function of ρ and about $(0.25\ \bar{n}_e)^{1/5}$ for $\rho \lesssim 1$ equ. (5) can be integrated analytically to

$$T_e(\rho) = T_e(o)\ \exp\ \left[-\frac{P_{OH}(a)}{C}\ \rho^2\ \left(1 - \frac{\alpha}{2}\ \rho^2\right)\right] \qquad (7)$$

the constant $C = 4\pi\ \chi_o\ B_\varphi\ \bar{n}_{14}^{1/5}\ q_a$.

In an earlier analysis of ohmically heated discharges of ASDEX /4/ it was found that the heating power P_{OH} scales as:

$$P_{OH} = B_1\ Z_{eff}^{1/2}\ \frac{(1 + 4.85\ \bar{n}_{14})}{q_a + 1}\ \cdot\ 380\ \frac{W}{cm}$$

where $B_1 = B\ /1\ T$; $n_{14} = n_e/10^{14}\ cm^{-3}$ and equ. (5) can be written as

$$T_e(\rho)/T_e(o) = \exp\ [-A\cdot q^*\cdot n^*\ \frac{D}{\chi_o}\ \rho^2(1 - \frac{\alpha}{2}\ \rho^2)] \qquad (8)$$

with $A = (Z_{eff}/B_1^{1/2}$; $q^* = q_a/(q_a+1)$; $n^* = (1+4.85\ \bar{n}_{14})/\bar{n}_{14}^{1/5}$;

$D = 2{,}33\cdot 10^3\ cm^2/s$ and $\alpha = 0.2$.

Equation (8) represents the shape of the temperature profile valid for the boundary region $0.9 \lesssim r/a \leq 1$ where ion heat conductivity is not significant. In fact the T_e-profiles of Fig. 6 can be described satisfactorily by equ.(8) with the central electron temperature $T_e(o)$ obtained from measured electron cyclotron emission, Z_{eff} calculated from T_e profiles and Spitzer-conductivity /8/ and $\bar{n}$ from microwave interferometry inserted in equ. (8). This is demonstrated by the solid lines in Fig. (6) for radii inside the separatrix. The electron heat diffusivity has been taken as stated before /6/:

$$\chi_e = \chi_o \cdot B_1/(n_{14}^{0,8} \cdot q \cdot T_1); \qquad \chi_o = (2 \pm 0.2) \cdot 10^3 \text{ cm}^2/\text{s}$$

The attempt to set $\chi_e \sim 1/n_{14}$ does not reproduce the measured T_e profiles; the exponent of n_{14} is clearly below unity!

In the open field line area $\Delta r > 0$ an exponential decay of the temperature profile was obtained. At the separatrix, naturally, the measured T_e values deviate from the theoretical curves (dotted lines, Fig. 6). This means physically that there exists a transition area of thickness $\Delta d \sim 0{,}5 \ldots 1$ cm as interface between the hot plasma core within the separatrix and the nearby scrape-off area with its different transport phenomena. Δd becomes smaller at low densities and consequently T_e profiles change more abruptly at the separatrix.

As the electron energy flux across the separatrix by heat conduction is assumed to be constant, it is surprising that T_e gradients $|\partial T_e/\partial r|$ become larger at $r > r_s$ in the scrape-off layer. Additional loss channels parallel to B would leave a smaller fraction of energy to be conducted perpendicular to B in the radial direction and hence the slope of the $T_e(r)$ function should decrease. The observed steepening of the T_e profile when the separatrix is crossed cannot be explained by errors of the measuring system, which means that either $\chi_e(r)$ changes essentially at $r = r_s$ or the existence of additional energy sources at the plasma edge close to the separatrix have to be postulated.

In case of neutral beam additional heating this observation can be made even more evident. This is demonstrated in Fig. 5a where the electron temperature is plotted against $\Delta r = r - r_s$ for the 3 typical cases.
1. ohmic heating alone, 2. neutral beam heating during the "L"-phase

(low β_p) and 3. during the "H" phase (high β_p). Within the separatrix $\Delta r < 0$ the $T_e(r)$ curves develop steadily and grow proportionally at all radii. In the scrape-off region $\Delta r > 0$ the enhanced steepening of the $T_e(r)$ curves is occurring. In the "OH" and the "L"-case of Fig. 5a temperatures rise about proportional at all radii. In the "H" case, however, the profile steepening at the separatrix drastically exceeds that of the OH and L curves. Calculation of the heat conductivities as estimated according to eq. (3) from the profile characteristics of Fig. 5a with P_{OH} substituted by $P_{OH} + P_{beam}$, at the location where $|\partial T_e/\partial r|$ takes a maximum, reveals that χ_e increases by a factor of ≈ 3 going from an OH to an L discharge and drops again to the value initially found for the OH case when H-discharge conditions are reached. This agrees with the statement, valid for the total plasma, that the global energy confinement time drops from about 60 ms to 20 ... 30 ms at the OH → L discharge transition but recovers again to 50 ... 60 ms in an H discharge.

5. Summary

Measurement of the electron temperature and density in the plasma boundary reveals a change of the profile shape at the separatrix $r=r_s$. For $r < r_s$ the profiles are strongly dependent on the core plasma parameters; the influence of these on the scrape-off parameters is weak, however; the characteristics of T_e and n_e profiles can be summarized as follows:

1. T_e and n_e profiles decay exponentially outside the magnetic separatrix. $\lambda_T = T/\frac{\partial T}{\partial r}$, the e-folding length of the electron temperature, is about 1 cm for ohmically heated discharges and drops to about 0.7 cm when 3 MW additional beam heating is applied; $\lambda_n = n_e/\frac{\partial n_e}{\partial r}$, the e-folding length of the density, is about 1,5 ... 2 cm for all discharges.

2. The electron temperature inside the separatrix, $r \lesssim r_s$, depends on the safety factor q_a and the plasma density (systematic dependencies on Z_{eff} or B_φ have not been studied) and can be represented by

$$T_e(r) = T_o \exp\left[-a_1 r^2 (1-a_2 r^2)\right] ; \qquad r \lesssim r_s$$

(see equ. (8), chapter 4) for ohmically heated plasmas. The electron heat conductivity scaling law:

$$\chi_e = \frac{\chi_o B_\varphi}{n_e^{0.8} q T_e}; \qquad \chi_o = (2 \pm 0.2) \cdot 10^3 \text{ cm}^2/\text{s}$$

(B_φ: T, n_e: 10^{14} cm^{-3}, T_e: keV) is valid at the plasma edge with closed magnetic field lines and negligible ion heat conduction. The separatrix temperature $T(r = r_s) \sim (0{,}08 \ldots 0{,}10) \cdot T_e(r = 0)$.
When additional beam heating is applied to an ohmic heated discharge, the electron temperature profiles rise about linearly with heating power inside the separatrix. The temperature at the separatrix, however, does never exceed 250 eV ($P \lesssim 3$ MW). Profile gradients outside the separatrix become very large when "H" discharge conditions are reached.

3. The electron density at the plasma edge inside the separatrix is proportional to $\bar{n}$, the line averaged density, up to $\bar{n} \lesssim 0{,}25 \cdot 10^{14}$ cm^{-3} but rises faster than linear at higher densities since $n_e(r)$ profiles become broader. When Ti-getter pumps are in action no deviation from linearity can be observed but the edge density becomes smaller. Generally the separatrix density is related to the line averaged density as:

$$n_e(r = r_s) \approx (0.2 \ldots 0{,}3)\, \bar{n}_e.$$

When neutral beam injection is applied, a drop of the edge density is generally observed as consequence of a deterioration of particle confinement; however, the n_e-profiles recover again when "H"-discharge conditions and high β_p values are reached.

Acknowledgement

The authors express their thanks to the entire ASDEX team, especially to Dr. Keilhacker, Dr. Klüber and Dr. E. Meservey for helpful discussions.

References

/1/ Quantel, Orsay, France.

/2/ Mahdavi, M.A., Applied Optics 16 (1977), 1765.

/3/ EMI Electron Tubes Ltd., London U.K.

/4/ Klüber, O., Murmann, H., IPP Report III/72 (1982).

/5/ Keilhacker, M. et al. "Plasma Boundary Layer in Limiter Divertor Tokamaks", International Conference on Plasma Physics (IAEA) Göteborg, Sweden.

/6/ Coppi, B., Mazzucato, E., Physics Letters 71 A, 4 (1979)

/7/ Müller, R., Behringer, K., Niedermeyer, H., Nucl. Fus. 22, 12 (1982)

/8/ Eberhagen, A., private communication
Kissel, S., IPP Report III/94

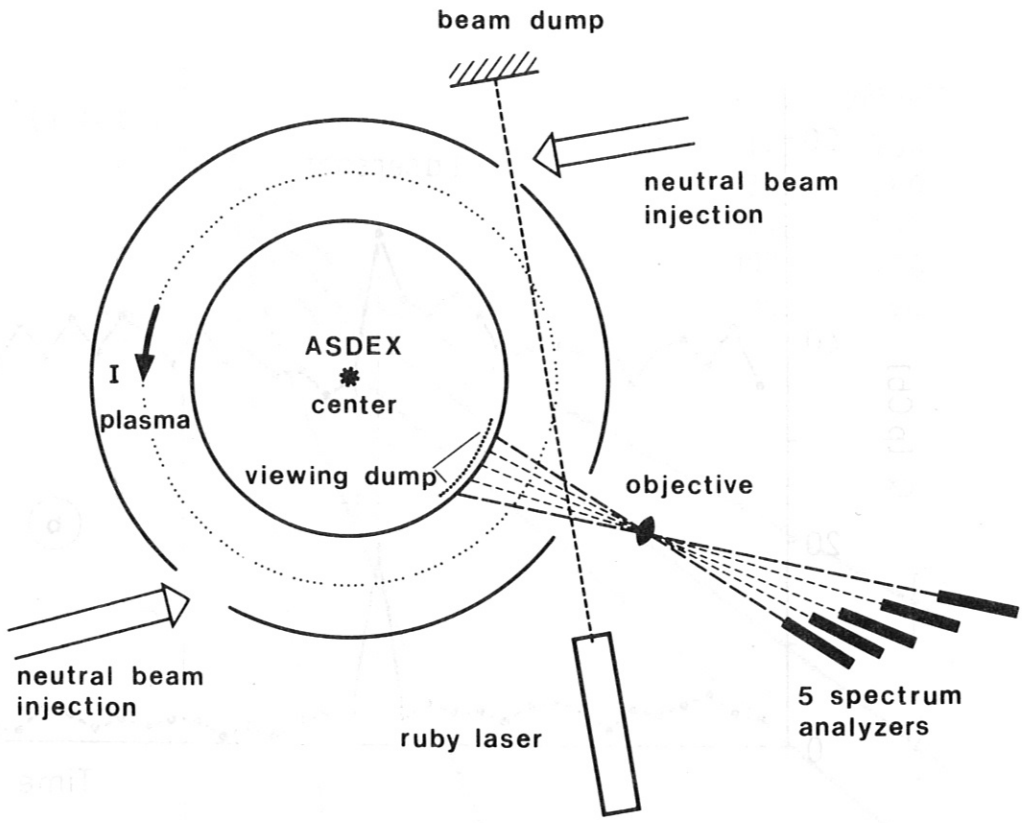

Fig. 1: Schematic set-up of the Thomson scattering system in the plasma boundary of ASDEX.

Laser:	6943 Å, 20 ns, 12 J, $\lesssim$1 mrad
Spectrum analysers:	interference filter/polarizing optics, 3 spectral channels per point
Location:	equatorial plane 200 cm $\leq$ R $\leq$ 206 cm; $0{,}87 \leq r/a \leq 1{,}03$; $\Delta r \sim 1$ cm; 5 local points-simultaneous measurement
Range:	2 eV $\leq T_e \leq$ 1 keV; $n_e \geq 5 \cdot 10^{11}$ cm^{-3}

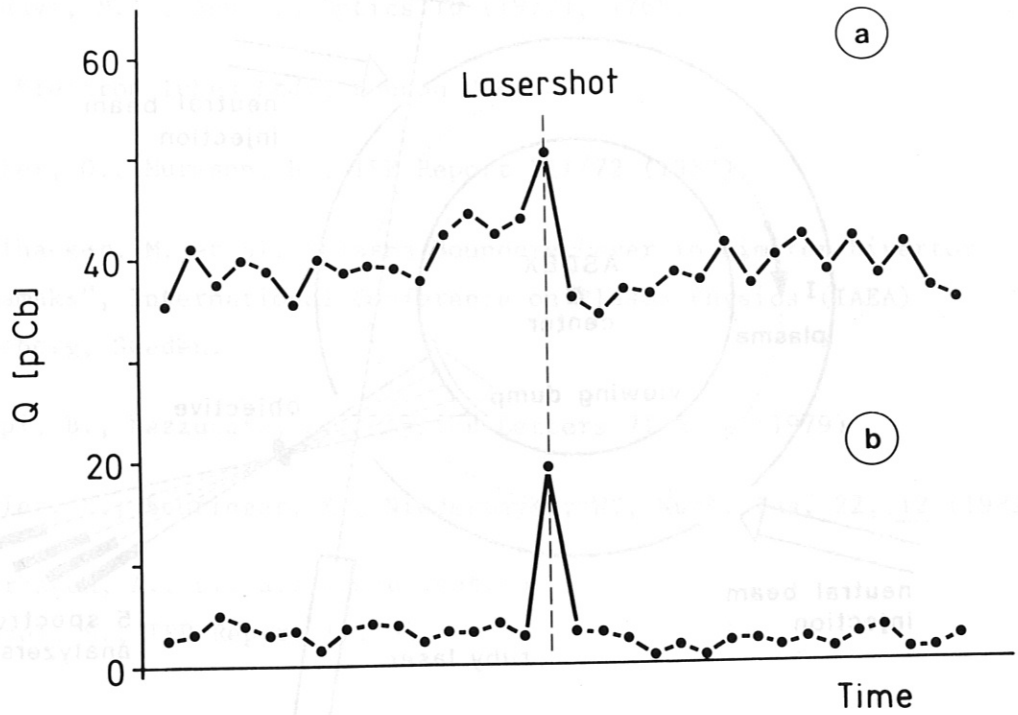

Fig. 2: Integrated photomultiplier output current $Q = \int_{\Delta t} Jdt$, as measured during 32 time intervals of 60 ns width before, during and after the laser pulse by two of 15 CAMAC ADC's at low signal level (b) and at the detection limit (a).

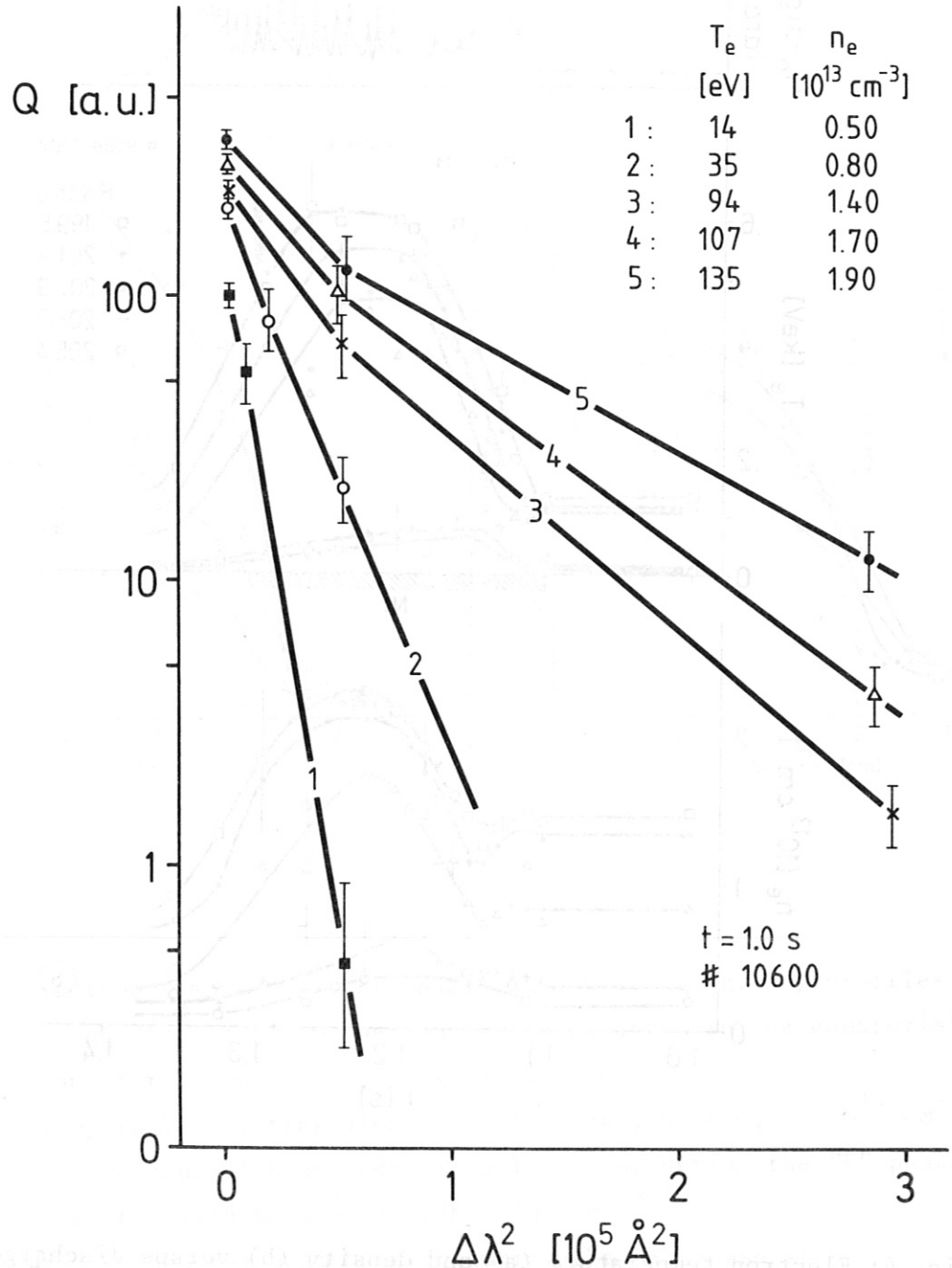

Fig. 3: Typical spectra: the photomultiplier output charge versus $\Delta\lambda^2$ of five spectrum analysers for an ohmically heated discharge. $\Delta\lambda$ is the spectral distance of an interference filter channel from the laser wave length.

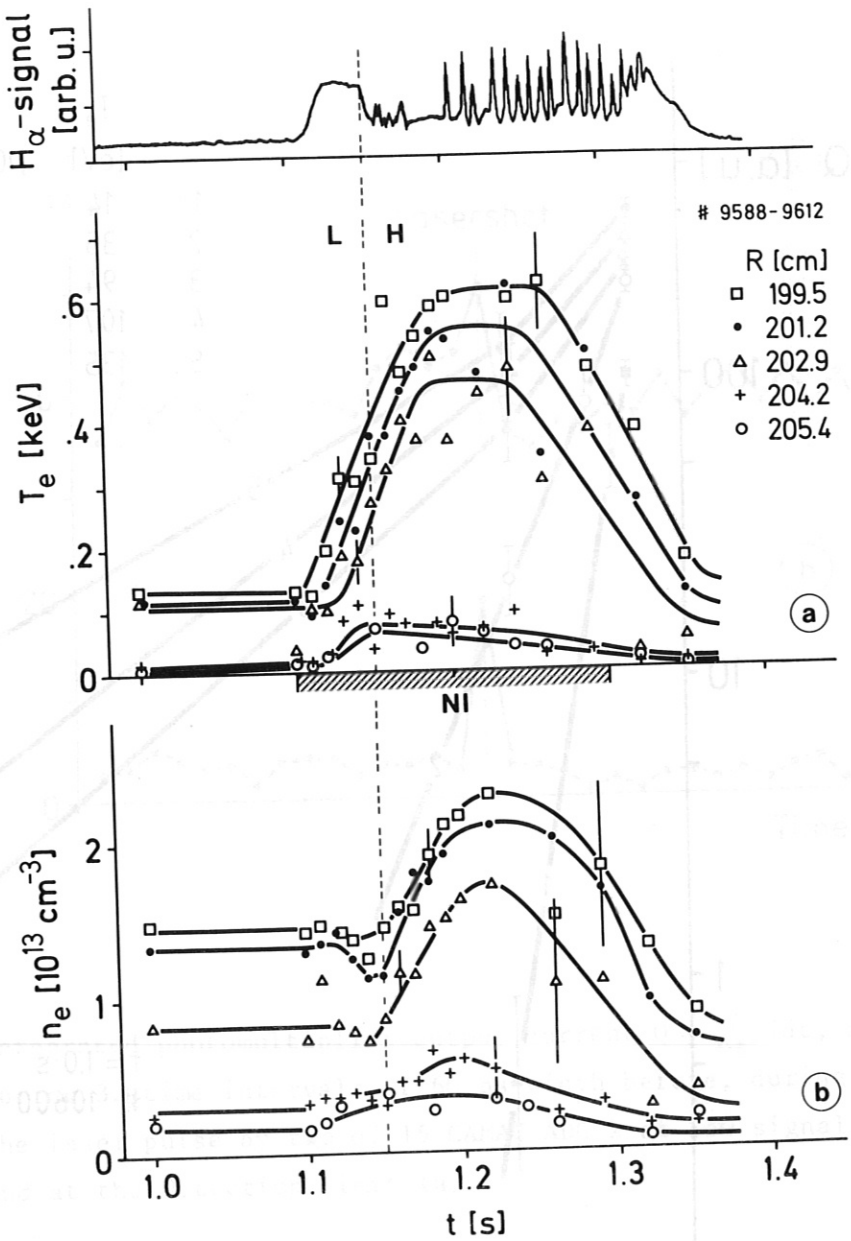

Fig. 4: Electron temperature (a) and density (b) versus discharge time for 5 locations in the plasma edge. Neutral beam heating occurs between 1.1 and 1.3 sec. The H_α radiation intensity from the divertor chamber is depicted in the same time scale (top). It is characterized by a sharp drop when the L → H transition occurs. At the onset of H_α light bursts (t ~ 1.2 sec) the plasma becomes violent which is reflected in a drastic increase of scattering of the T_e and n_e data.

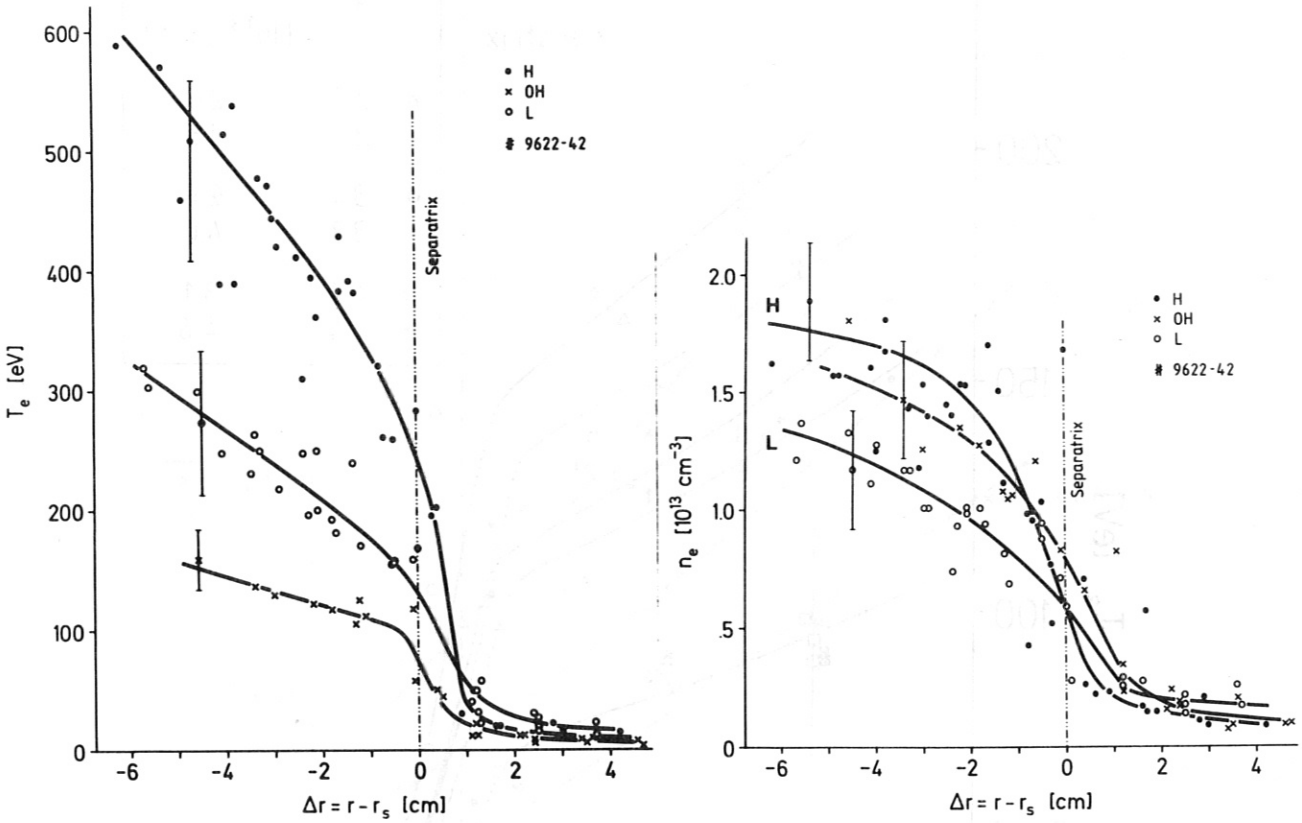

Fig. 5: Electron temperature (Fig. 5a) and density (Fig. 5b) profiles versus distance from the magnetic separatrix in the equatorial plane for 3 typical discharge conditions:

x: ohmically heating alone; t = 1.05 sec, $\bar{n}_e = 0{,}4 \cdot 10^{14}$ cm^{-3}

o: 3 MW neutral beam (additional) heating during the "L" phase at t = 1.15 sec, $\bar{n}_e = 0{,}38 \cdot 10^{14}$ cm^{-3}

●: 3 MW neutral beam heating during the "H" phase at t = 1.25 sec, $\bar{n}_e = 0{,}47 \cdot 10^{14}$ cm^{-3}

I = 320 kA; B_φ = 2.17 T

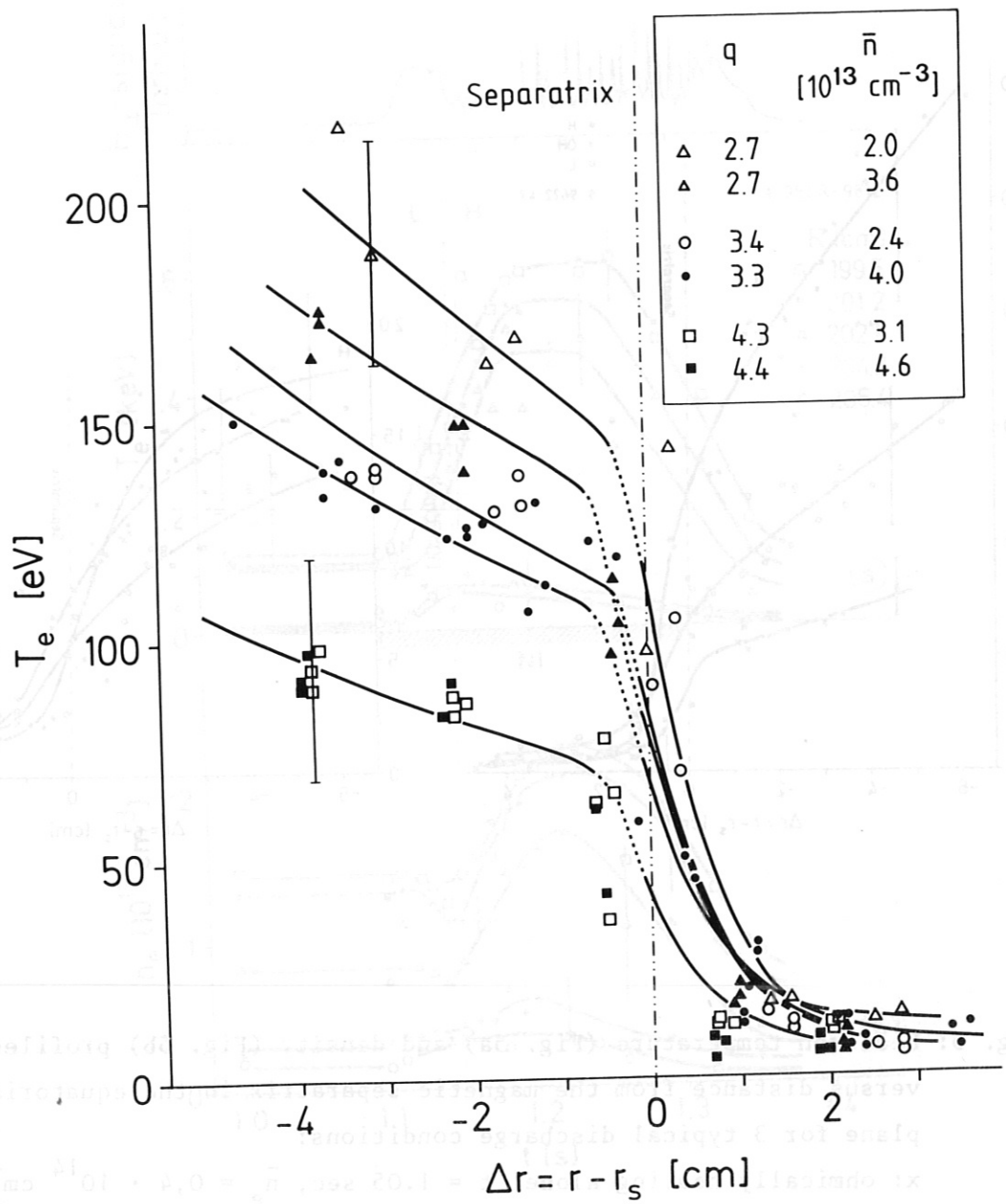

Fig. 6: Electron temperature in the plasma boundary versus distance from the magnetic separatrix for ohmically heated discharges with different q and $\bar{n}$ values. The solid lines inside the separatrix are calculated according to equ. (8). Outside the separatrix an exponential decay function was assumed.

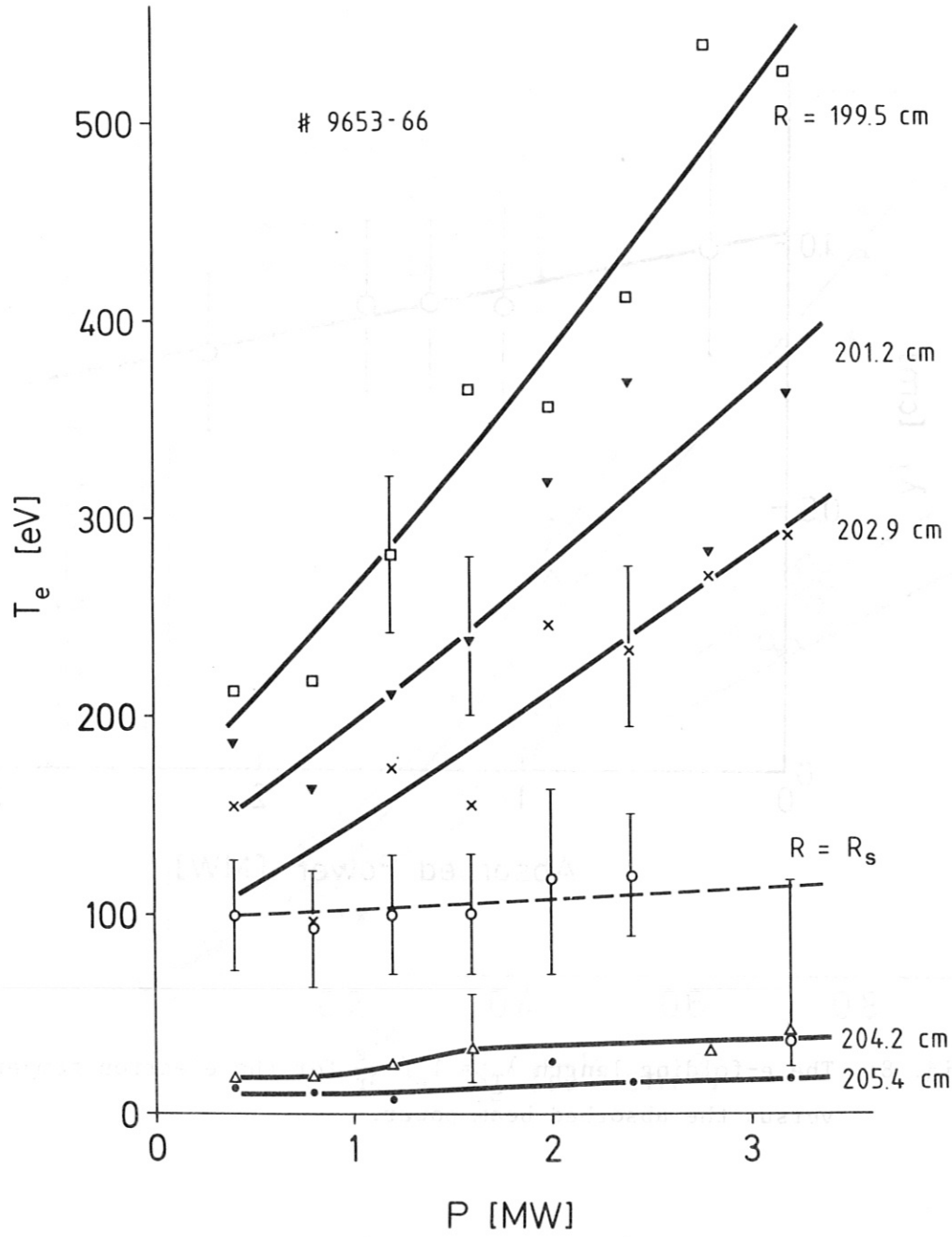

Fig. 7: Electron temperature during neutral beam heating in the "L"-phase versus the absorbed beam power (solid lines) at different radial positions, and separatrix temperature $T_e(R = R_s)$ (dashed line). For this low q discharge (q = 2.7) $T_e(R_s)$ is almost constant.

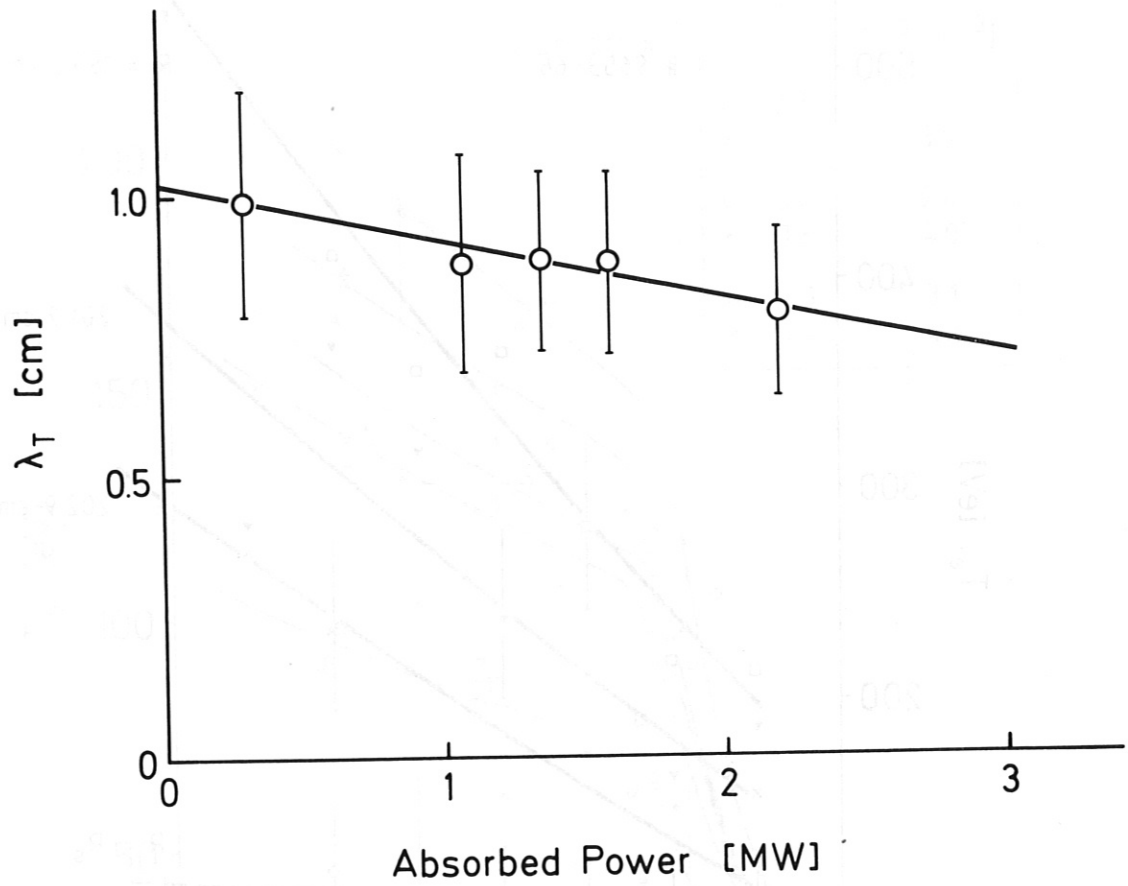

Fig. 8: The e-folding length $\lambda_T = T_e / \frac{\partial T_e}{\partial r}$ for the electron temperature versus the absorbed beam power.

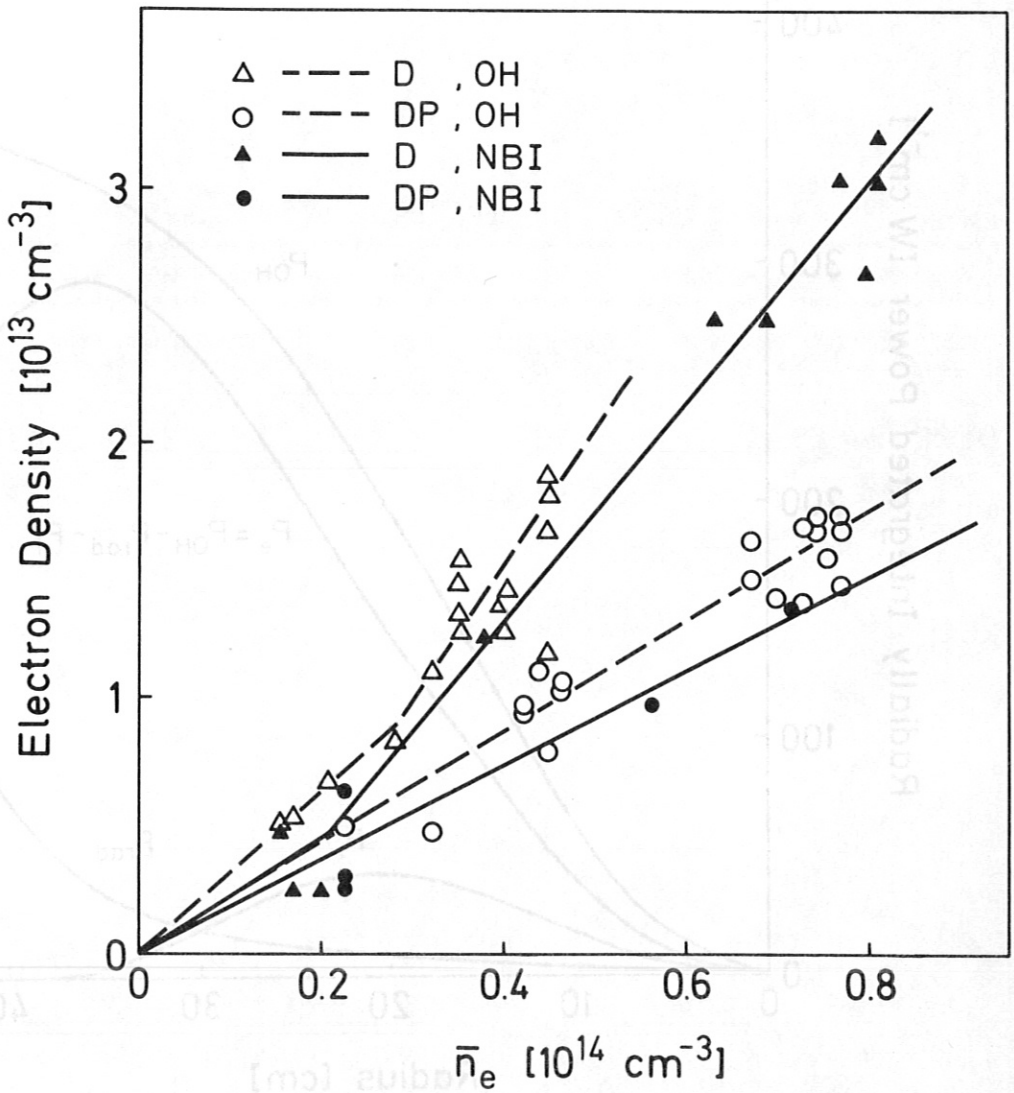

Fig. 9: Electron densities at radii (r_s - 1 cm) $\lesssim r \lesssim r_s$ slightly inside the separatrix versus the line averaged density $\bar{n}_e$ for different discharge conditions.

D: Divertor discharge

DP: Divertor discharge with Ti-gettering

OH: Ohmic heating

NBI: Ohmic heating and neutral beam heating

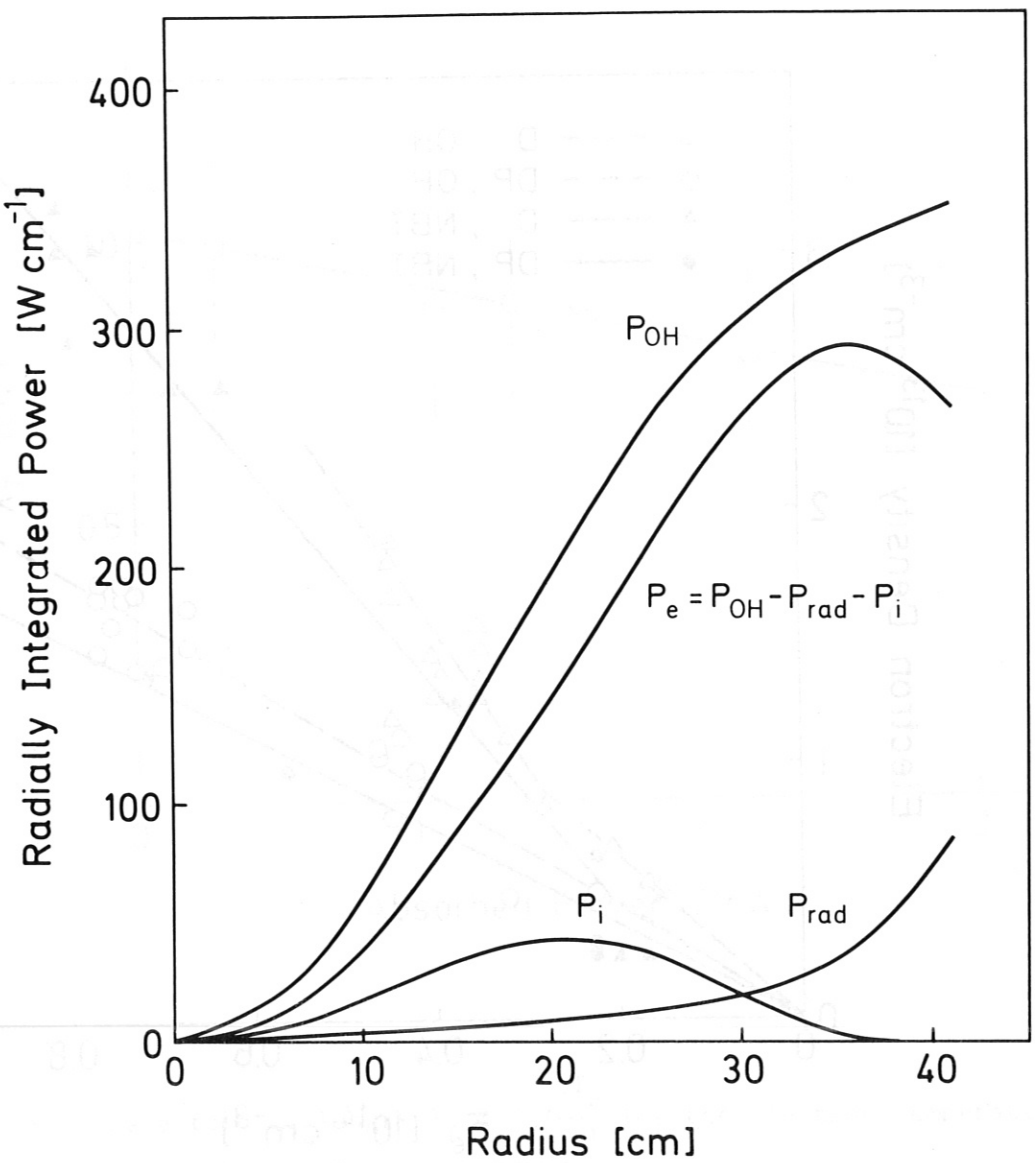

Fig.10: The radially integrated power balance for a typical ohmically heated discharge. $\bar{n}_e = 0{,}28 \cdot 10^{14}$ cm^{-3}; $q_a = 4{,}2$; $B_\varphi = 2{,}17$ T

P_{OH} : ohmic heating power

P_i : power dissipated by ion heat conduction

P_{rad} : radiated power as measured by bolometry

$P_e = P_{OH} - P_i - P_{rad}$: power dissipated by electron heat conduction